Broadband Characterization of Materials Using a Dual-Ridged Waveguide

Milo W. Hyde IV, *Senior Member, IEEE,* Michael J. Havrilla, *Senior Member, IEEE,* Andrew E. Bogle, *Member, IEEE,* and Nathan J. Lehman

***Abstract*—A transmission/reflection material characterization technique that uses dual-ridged waveguides is presented. The proposed dual-ridged-waveguide system combines many of the positive aspects of traditional transverse electromagnetic-mode (e.g., coaxial, free space, and stripline) and rectangular waveguide systems, i.e., broadband measurements and accurate calibration. A brief discussion on the derivation of the theoretical scattering parameters, required for the extraction of permittivity and permeability of a material under test, is provided. Two methods for computing the cutoff wavenumber of the dual-ridged waveguide—essential to the material characterization process—are also discussed. The first, which utilizes the mode-matching technique, is applicable to dual-ridged-waveguide apertures composed of right-angled corners. The second uses the surface equivalence principle and a magnetic-field integral equation formulation to find the cutoff wavenumber. This approach is applicable to dual-ridged waveguides with rounded corners, which often result from the dual-ridged waveguide manufacturing process. Thus, for the first time, the effect of rounded dual-ridged-waveguide aperture corners on the measurement of permittivity and permeability is assessed. Experimental material characterization results of a magnetic absorbing material are presented and analyzed to validate the proposed technique. An extensive error analysis on the extracted values of permittivity and permeability is also performed by taking into account manufacturer-specified dual-ridged-waveguide design tolerances as well as uncertainties in sample position, sample thickness, sample-holder length, and measured scattering parameters.**

***Index Terms*—Integral equations, measurement uncertainty, microwave measurements, moment methods, permeability measurement, permittivity measurement, uncertainty, waveguides.**

I. Introduction

DETERMINING the relative permittivity ε_r and permeability μ_r of materials at microwave frequencies is used in the defense, aerospace, industrial, and scientific communities. For the past several decades, transmission/reflection (TR) RF material characterization techniques have been developed using rectangular waveguides (WGs) [1]–[12], coaxial transmission lines [12]–[21], free-space systems [12], [22], [23], and stripline systems [12], [24], [25]. Note that a very good review of TR material characterization techniques is given in [26]. Coaxial, free-space, and stripline systems, being measurement geometries which support transverse electromagnetic (TEM)-mode propagation, offer broadband ε_r and μ_r results; however, sample preparation (i.e., required specimen sizes for free-space systems and machining requirements for coaxial and stripline systems) and system calibration can be difficult. On the other hand, rectangular WG measurement geometries can be calibrated easily and accurately (e.g., thru-reflect-line (TRL) calibration [27]), and specimen size and machining requirements are typically more relaxed than free-space, coaxial, or stripline systems. Rectangular WG systems do not support TEM-mode propagation and therefore are bandlimited between the cutoff frequencies of the dominant mode and the first higher order mode (typically, TE_{10} and TE_{20} modes), respectively.

In this paper, a TR material characterization technique that uses dual-ridged waveguides (DRWGs) is presented. The proposed DRWG measurement system combines many of the attractive features of TEM-mode and rectangular WG systems, i.e., broadband measurements and accurate calibration. A schematic of the TR DRWG measurement geometry is shown in Fig. 1. Section II describes two methods (both used in the analysis to follow) for calculating the cutoff wavenumber k_c of the DRWG. The first uses the mode-matching technique and is only applicable to DRWG apertures composed of right-angled corners. It is highly accurate and converges quickly. The second technique utilizes the surface equivalence principle and a magnetic-field integral equation (MFIE) formulation to find k_c. While not as quick to converge as the first technique, the MFIE formulation method can be used to find the k_c of DRWGs with rounded aperture corners. Since the aperture corners are rounded in the DRWG manufacturing process, utilization of the MFIE formulation approach permits, for the first time, an assessment of the effect that rounded corners have on the measurement of ε_r and μ_r.

In addition to the descriptions of the two methods to determine k_c, a brief summary on the derivation of the theoretical scattering parameters (S-parameters), ultimately necessary to determine ε_r and μ_r of the material under test (MUT), is also

Manuscript received November 13, 2012; revised January 16, 2013; accepted February 25, 2013. Date of publication July 4, 2013; date of current version November 6, 2013. The Associate Editor coordinating the review process was S. Kharkovsky.

M. W. Hyde IV, M. J. Havrilla, and N. J. Lehman are with the Department of Electrical and Computer Engineering, Air Force Institute of Technology, Wright-Patterson Air Force Base, Dayton, OH 45433 USA (e-mail: milo.hyde@us.af.mil; michael.havrilla@afit.edu; nathan.lehman@afit.edu).

A. E. Bogle is with the Department of Electrical and Computer Engineering, Air Force Institute of Technology, Wright-Patterson Air Force Base, Dayton, OH 45433 USA, and also with the Sensor Systems Division, University of Dayton Research Institute, Dayton, OH 45469 USA (e-mail: andrew.bogle.ctr.ca@afit.edu).

Color versions of one or more of the figures in this paper are available online at http://ieeexplore.ieee.org.

Digital Object Identifier 10.1109/TIM.2013.2270050

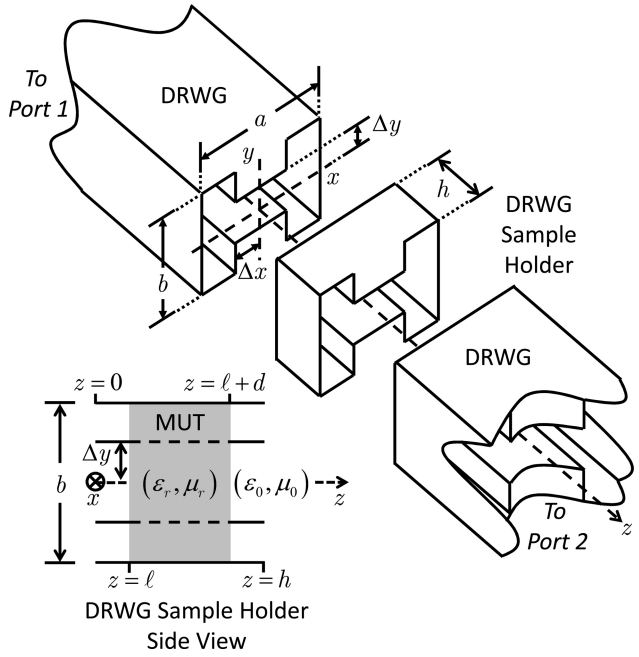

Fig. 1. TR DRWG measurement geometry. The figure depicts two air-filled DRWGs connected to a DRWG sample-holder section (of length h) which contains the MUT (of thickness d). For error analysis purposes, an air spacing (of length ℓ) between the origin and the MUT is included to model the possibility that the front face of the MUT is not aligned with the $z = 0$ plane (i.e., the calibration plane). The MUT is assumed to fully fill the cross section of the DRWG and therefore DRWG dominant-mode propagation is assumed throughout.

provided. In Section III, experimental material characterization results of a magnetic absorbing material are presented and analyzed to validate the proposed measurement geometry. An extensive error analysis on the extracted values of ε_r and μ_r is performed by taking into account manufacturer-specified DRWG design tolerances, i.e., aperture width a, aperture height b, gap width Δx, gap height Δy, and corner curvature, as well as uncertainties in sample position ℓ, sample thickness d, sample-holder length h, and measured S-parameters. Finally, this paper is concluded with a summary of the contributions.

II. Methodology

Consider the TR DRWG measurement geometry shown in Fig. 1. The figure depicts two air-filled DRWGs connected to a DRWG sample-holder section (of length h) that contains the MUT (of thickness d). For error analysis purposes, an air gap (of length ℓ) between the origin and the MUT is included in the development to model the possibility that the front face of the MUT is not aligned with the $z = 0$ plane (i.e., the calibration plane). The MUT is assumed to fully fill the cross section of the DRWG and therefore DRWG dominant mode, commonly termed a TE^z_{10} hybrid mode [28], [29], propagation is assumed throughout.

The ε_r and μ_r of the MUT are found by first deriving theoretical expressions for the reflection, S_{11}^{thy} and S_{22}^{thy}, and transmission, S_{21}^{thy} and S_{12}^{thy}, coefficients. Expressions for these coefficients are found by enforcing continuity of the transverse fields at the front and back faces of the MUT. These quantities take the common form [30], [31]

$$\begin{aligned} S_{11}^{\mathrm{thy}} &= S_{22}^{\mathrm{thy}} = \frac{\Gamma\left(1-P^2\right)}{1-\Gamma^2P^2} \\ S_{21}^{\mathrm{thy}} &= S_{12}^{\mathrm{thy}} = \frac{P\left(1-\Gamma^2\right)}{1-\Gamma^2P^2} \end{aligned} \tag{1}$$

where $\Gamma = (Z - Z_0)/(Z + Z_0)$ is the interfacial reflection coefficient and $P = \exp(-jk_z d)$. Here, $Z = \omega\mu/k_z$ and $Z_0 = \omega\mu_0/k_{z0}$ are the DRWG dominant-mode wave impedances for the MUT-filled and air-filled DRWG regions, respectively. The factors $k_z = \sqrt{\omega^2\varepsilon\mu - k_c^2} = \sqrt{k^2 - k_c^2}$ and $k_{z0} = \sqrt{\omega^2\varepsilon_0\mu_0 - k_c^2} = \sqrt{k_0^2 - k_c^2}$ are the DRWG dominant-mode propagation constants for the MUT-filled and air-filled DRWG regions, respectively. Finally, k_c is the dominant-mode cutoff wavenumber of the DRWG. In the sections to follow, two methods, the mode-matching technique and an MFIE formulation, for obtaining its value are presented. Note that these two methods were chosen because they are the most applicable to the problem of interest. Several other methods for analyzing DRWGs exist [32]–[36].

A. Mode-Matching Method

The first method for obtaining k_c follows the methodology used by Montgomery [28] and Elliot [37] and later by Rong and Zaki [38] for more complicated ridged WGs. It involves expanding the fields in each DRWG subregion (i.e., the gap, $|x| \le \Delta x$, and trough, $|x| \ge \Delta x$, subregions) in a set of TE^z or TM^z modes [39], [40]. Note that the DRWG dominant mode is a TE^z mode; therefore, only the TE^z mode development is implicated here. The mode-matching technique [41] is then used to satisfy the continuity of transverse fields at $x = \Delta x$ and $-\Delta x$ yielding the following eigenvalue equations for k_c:

$$\begin{aligned} &\alpha_{\tilde{n}}\frac{\tan\left(k_{x\tilde{n}}^{\mathrm{g}}\Delta x\right) - \cot\left(k_{x\tilde{n}}^{\mathrm{g}}\Delta x\right)}{2k_{x\tilde{n}}^{\mathrm{g}}} \\ &+\beta_{\tilde{n}}\frac{\tan\left(k_{x\tilde{n}}^{\mathrm{g}}\Delta x\right) + \cot\left(k_{x\tilde{n}}^{\mathrm{g}}\Delta x\right)}{2k_{x\tilde{n}}^{\mathrm{g}}} \\ &\quad -\sum_{n,m}\alpha_n\frac{\psi_{m,n}\psi_{m,\tilde{n}}\cot\left[k_{xm}^{\mathrm{t}}\left(\frac{a}{2}-\Delta x\right)\right]}{k_{xm}^{\mathrm{t}}\frac{b}{2}\left(1+\delta_{m,0}\right)\Delta y\left(1+\delta_{\tilde{n},0}\right)} = 0 \\ &\alpha_{\tilde{n}}\frac{\tan\left(k_{x\tilde{n}}^{\mathrm{g}}\Delta x\right) + \cot\left(k_{x\tilde{n}}^{\mathrm{g}}\Delta x\right)}{2k_{x\tilde{n}}^{\mathrm{g}}} \\ &+\beta_{\tilde{n}}\frac{\tan\left(k_{x\tilde{n}}^{\mathrm{g}}\Delta x\right) - \cot\left(k_{x\tilde{n}}^{\mathrm{g}}\Delta x\right)}{2k_{x\tilde{n}}^{\mathrm{g}}} \\ &\quad -\sum_{n,m}\beta_n\frac{\psi_{m,n}\psi_{m,\tilde{n}}\cot\left[k_{xm}^{\mathrm{t}}\left(\frac{a}{2}-\Delta x\right)\right]}{k_{xm}^{\mathrm{t}}\frac{b}{2}\left(1+\delta_{m,0}\right)\Delta y\left(1+\delta_{\tilde{n},0}\right)} = 0 \end{aligned} \tag{2}$$

where

$$\begin{aligned} \psi_{m,n} &= \frac{1}{2}\left(\frac{1}{k_{yn}^{\mathrm{g}} - k_{ym}^{\mathrm{t}}} - \frac{1}{k_{yn}^{\mathrm{g}} + k_{ym}^{\mathrm{t}}}\right) \\ &\left\{\sin\left[k_{ym}^{\mathrm{t}}\left(\frac{b}{2}-\Delta y\right)\right] - (-1)^n\sin\left[k_{ym}^{\mathrm{t}}\left(\frac{b}{2}+\Delta y\right)\right]\right\}; \end{aligned} \tag{3}$$

n and $\tilde{n}$ represent basis and testing indices, respectively; $k_{ym}^{\mathrm{t}} = m\pi/b$ and $k_{yn}^{\mathrm{g}} = n\pi/(2\Delta y)$ are the y-directed DRWG

wavenumbers in the trough and gap subregions, respectively; k_{xm}^{t} and k_{xn}^{g} are the unknown x-directed DRWG wavenumbers in the trough and gap subregions, respectively, and α_n and β_n are the unknown complex TE^z modal amplitudes. Recall that $k_{z0} = \sqrt{k_0^2 - k_c^2} = \sqrt{k_0^2 - \left(k_{ym}^{\mathrm{t}}\right)^2 - \left(k_{xm}^{\mathrm{t}}\right)^2} = \sqrt{k_0^2 - \left(k_{yn}^{\mathrm{g}}\right)^2 - \left(k_{xn}^{\mathrm{g}}\right)^2}$; thus, at cutoff ($k_{z0} = 0$), (2) is of the form

$$\mathbf{A}\left(k_c\right)\begin{pmatrix}\boldsymbol{\alpha}\\ \boldsymbol{\beta}\end{pmatrix} = \begin{pmatrix}A_{11}\left(k_c\right) & A_{12}\left(k_c\right)\\ A_{21}\left(k_c\right) & A_{22}\left(k_c\right)\end{pmatrix}\begin{pmatrix}\boldsymbol{\alpha}\\ \boldsymbol{\beta}\end{pmatrix} = \mathbf{0} \tag{4}$$

where A_{11}, A_{12}, A_{21}, and A_{22} are $N \times N$ submatrices with A_{12} and A_{21} being diagonal. The cutoff wavenumber k_c is found by forcing an eigenvalue of $\mathbf{A}\left(k_c\right)$ to equal zero via numerical root search; $\begin{pmatrix}\boldsymbol{\alpha} & \boldsymbol{\beta}\end{pmatrix}^{\mathrm{T}}$ is the associated eigenvector of that zero eigenvalue. There are an infinite number of wavenumbers that satisfy (4) each corresponding to a distinct TE^z DRWG mode. The k_c which corresponds to the first zero of (4) is the dominant DRWG mode.

This method for obtaining k_c is simple and highly accurate. Since this method employs a basis set which is very similar in form to the actual behavior of the fields in the DRWG, only a small number of expansion modes (gap and trough modes) are required to obtain highly accurate k_c estimates [28]. Furthermore, analytical DRWG field expressions can be readily obtained once k_c and $\begin{pmatrix}\boldsymbol{\alpha} & \boldsymbol{\beta}\end{pmatrix}^{\mathrm{T}}$ have been determined. A major drawback of this approach is that it is limited to DRWG apertures composed of right-angled corners. This, of course, is not realistically possible. Indeed, as a result of the typical manufacturing process used to produce DRWGs, the corners are rounded. This is clearly shown in Fig. 2, where the inner and outer corners have a discernible curvature—r_1 and r_2, respectively. The effect of rounded corners on ε_r and μ_r extraction could be quite significant when one considers the behavior of the fields in a DRWG. A depiction of the dominant DRWG electric-field magnitude is shown in Fig. 3. Note the significant fringing of the fields around the gap subregion. This fringing is so pronounced because electric charge, deposited by the current traveling along the walls, builds up at the right-angled corners. Rounded corners present much less of an impediment to the current than right-angled corners and therefore less electric charge builds up at the boundaries between the gap and trough subregions subsequently affecting field fringing. To be able to understand and quantify how rounded corners (as well as uncertainties in the other DRWG dimension specifications) affect the reliability of ε_r and μ_r measurements obtained using a DRWG system, another method for finding k_c (in addition to the one just described) needs to be utilized.

B. MFIE Formulation Method

The second method for obtaining k_c utilized here follows the works of Swaminathan *et al.* [42], [43] and Kim *et al.* [44] who used the surface equivalence principle [40], [45], [46] and an integral equation formulation to find the natural modes of guiding structures. Later, Sun and Balanis [29], [47] applied this method specifically to ridged WGs.

In accordance with the surface equivalence principle, the PEC DRWG boundaries are replaced with an electric current

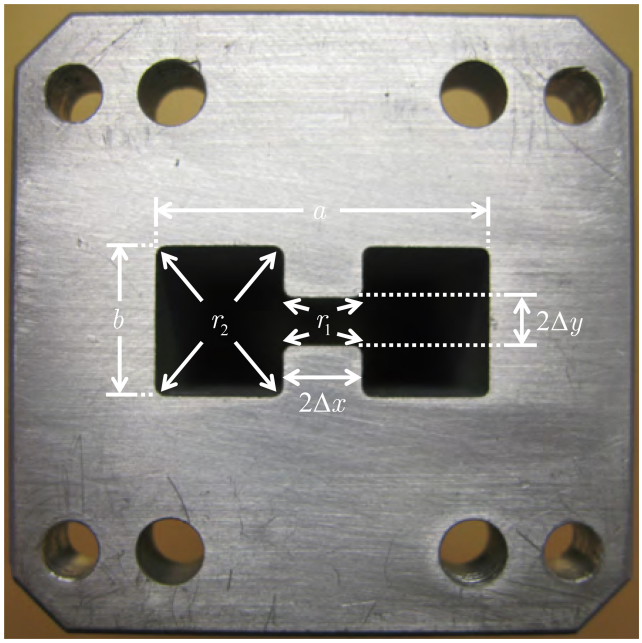

Fig. 2. Aperture photograph of the MEC WRD650 DRWG used in this research. The nominal values and tolerances for a, b, $2\Delta x$, $2\Delta y$, r_1, and r_2 are given in Table I.

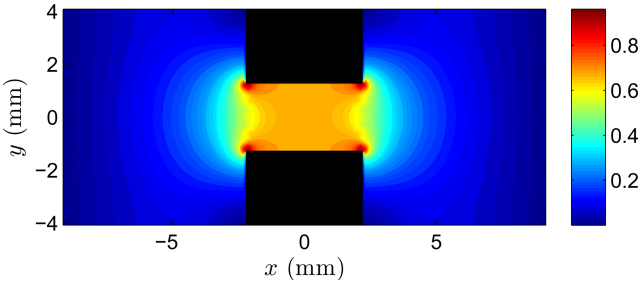

Fig. 3. Dominant DRWG electric-field magnitude. This depiction of the dominant mode was generated using five gap and 25 trough modes.

$\boldsymbol{J}$ which maintains the fields inside the structure. The magnetic field in the DRWG at cutoff can be found by utilizing this current and the free-space Green's function, namely

$$\boldsymbol{H}\left(\boldsymbol{\rho}\right) = \nabla_t \times \int_C \boldsymbol{J}\left(\boldsymbol{\rho}'\right)\frac{H_0^{(2)}\left(k_c\left|\boldsymbol{\rho} - \boldsymbol{\rho}'\right|\right)}{\mathrm{j}4}dC' \tag{5}$$

where $\boldsymbol{\rho} = \hat{\boldsymbol{x}}x + \hat{\boldsymbol{y}}y$ is the observation vector, $\boldsymbol{\rho}' = \hat{\boldsymbol{x}}x' + \hat{\boldsymbol{y}}y'$ is the source vector, and C is the contour traced out by the DRWG boundaries. Note that the 2-D form of the free-space Green's function is utilized here because the cross section of the DRWG does not change and, at cutoff, there is no z variation in the field ($k_z = 0$). Utilizing the PEC magnetic-field boundary condition, viz.,

$$\hat{\boldsymbol{n}}\left(\boldsymbol{\rho}\right) \times \boldsymbol{H}\left(\boldsymbol{\rho}\right) = \boldsymbol{J}\left(\boldsymbol{\rho}\right) \quad \boldsymbol{\rho} \in C \tag{6}$$

where $\hat{\boldsymbol{n}}$ is the unit normal pointing into the field region (i.e., into the DRWG), and separating (6) into transverse $\hat{\boldsymbol{t}} = \hat{\boldsymbol{x}}\cos\Omega\left(\boldsymbol{\rho}\right) + \hat{\boldsymbol{y}}\sin\Omega\left(\boldsymbol{\rho}\right)$ and longitudinal $\hat{\boldsymbol{z}}$ components

yields two uncoupled MFIEs

$$\begin{aligned} 0 &= J_t(\boldsymbol{\rho}) + \mathrm{j}\frac{k_c}{4}\int_C \frac{y-y'}{R}\cos\Omega(\boldsymbol{\rho}')\, J_t(\boldsymbol{\rho}')\, H_1^{(2)}(k_c R)\, dC' \\ &\quad -\mathrm{j}\frac{k_c}{4}\int_C \frac{x-x'}{R}\sin\Omega(\boldsymbol{\rho}')\, J_t(\boldsymbol{\rho}')\, H_1^{(2)}(k_c R)\, dC' \quad \boldsymbol{\rho}\in C \\ 0 &= J_z(\boldsymbol{\rho}) + \mathrm{j}\frac{k_c}{4}\int_C \frac{y-y'}{R}\cos\Omega(\boldsymbol{\rho})\, J_z(\boldsymbol{\rho}')\, H_1^{(2)}(k_c R)\, dC' \\ &\quad -\mathrm{j}\frac{k_c}{4}\int_C \frac{x-x'}{R}\sin\Omega(\boldsymbol{\rho})\, J_z(\boldsymbol{\rho}')\, H_1^{(2)}(k_c R)\, dC' \quad \boldsymbol{\rho}\in C \end{aligned} \tag{7}$$

where $R = |\boldsymbol{\rho} - \boldsymbol{\rho}'|$, and $\Omega(\boldsymbol{\rho}) = \mathrm{Tan}^{-1}(\rho_y/\rho_x)$ is the angle between $\boldsymbol{\rho}$ and the x-axis (Tan^{-1} is the four-quadrant inverse tangent function) [46]. It should be noted that to arrive at the forms for the MFIEs in (7) required bringing the derivatives contained in ∇_t inside the integrals. At cutoff, a TE^z mode supports only a transverse current; therefore, the first MFIE is relevant here [29]. Note that the other MFIE (the longitudinal current MFIE) can be used to find the cutoff wavenumbers of TM^z modes [29].

Solving the transverse current MFIE in (7) can be accomplished using the Method of Moments [46], [48]. At least, first-order differentiability is required for basis and testing functions to overcome the Green's function source-point singularity [46]; thus, pulse basis and delta testing functions (point matching) will suffice. Note that an electric-field integral equation formulation could also have been employed; however, the presence of the $\nabla_t\nabla_t\cdot$ operator would have required a higher order and thus a more complex set of basis and testing functions to overcome the source-point singularity. Expanding J_t in pulse basis functions, testing with delta functions, and subsequent simplification yields a matrix equation $\mathbf{Z}(\mathbf{k_c})\boldsymbol{I} = \mathbf{0}$, where, like in the mode-matching method, k_c is found by forcing an eigenvalue of the impedance matrix $\mathbf{Z}$ to zero via numerical root search. The electric current $\boldsymbol{I}$ is the associated eigenvector of that zero eigenvalue from which the field can be computed.

Like the mode-matching method described previously, the MFIE formulation method is rather simple; however, it is not as accurate as the mode-matching technique. The reason for this is the choice of expansion functions (a series of pulses, in this case) which do not accurately model the true nature of the electric current. Therefore, a large number of pulses are required to obtain an accurate estimate of k_c making numerical computation more difficult. Furthermore, no analytical field expressions (the integrals in the field expressions must be calculated numerically) can be obtained using this method. However, a major advantage of this method over the mode-matching technique is that k_c can be computed for DRWGs with rounded corners; thus, the effect that rounded corners have on the measurement of ε_r and μ_r can be quantified via error analysis. For a DRWG aperture composed of right-angled corners, the two methods differ in k_c values by approximately 1%. When the DRWG aperture corners are rounded, the two methods differ in k_c values by approximately 3% using the DRWG specifications given in Table I. This 3% is quite significant when one considers that the parameter k_c is involved in the calculation of the propagation constant k_z, which is the most important quantity in determining S-parameter phase. A reliable S-parameter phase measurement is critical for accurate determination of ε_r and μ_r.

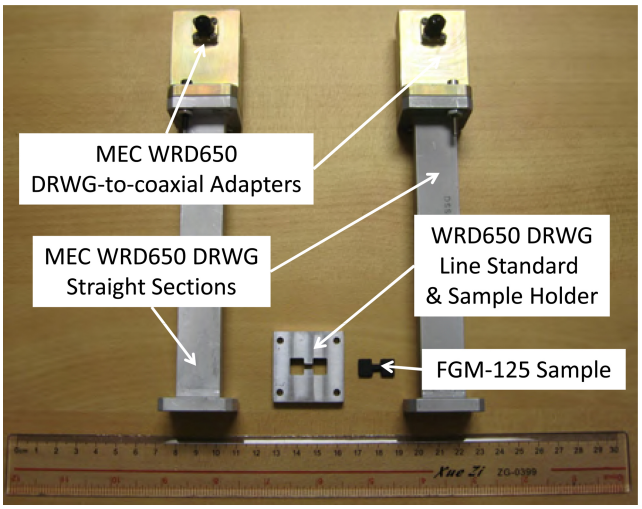

Fig. 4. WRD650 DRWG material measurement apparatus used in this experiment.

In the analysis presented and discussed in the following, a pulse basis function width of $\lambda/200$ was chosen for determining k_c for a DRWG aperture composed of right-angled corners. This width was selected because the value of k_c did not appreciably change for smaller pulse widths implying convergence. For a DRWG aperture composed of rounded corners, the pulse basis function width was chosen to be either $\lambda/200$ or the width required to fit a minimum of five pulses around the tightest DRWG aperture corner—whichever yielded the smaller width. This ensured that the curvature of every corner comprising the DRWG aperture was resolved and, most importantly, that the value obtained for k_c could be considered accurate.

III. Experimental Verification

In this section, experimental DRWG material characterization results are presented. Before analyzing the measurement results, a discussion of the measurement apparatus and procedure is warranted.

A. Apparatus Description and Experimental Procedure

Material characterization measurements were made at 6–18 GHz of ECCOSORB® FGM-125 (d = 3.12 mm) [49], a silicon-based lossy magnetic absorbing material, using an Agilent E8362B vector network analyzer (VNA) [50]. The TR DRWG measurement apparatus consisted of two Microwave Engineering Corporation (MEC) WRD650 DRWG-to-coaxial adapters [51] attached to two 15.24 cm DRWG straight sections [52]. In addition to the MEC WRD650 DRWGs, a locally machined h = 6.98 mm DRWG sample holder was used to hold the FGM-125 sample. A photograph of the pertinent parts of the DRWG measurement apparatus is shown in Fig. 4.

Before the material measurements were made, the apparatus was calibrated using a TRL calibration [27]. The custom made

TABLE I
MEC WRD650 DRWG DIMENSIONS AND TOLERANCES

	Dimension	Tolerance
a	18.288 mm	$\pm$0.0762 mm
b	8.1534 mm	$\pm$0.0762 mm
$2\Delta x$	4.3942 mm	$\pm$0.0254 mm
$2\Delta y$	2.5654 mm	$\pm$0.0254 mm
r_1	0.5588 mm	$\pm$0.05588 mm
r_2	0.254 mm	$\pm$0.254 mm

DRWG sample holder discussed previously and shown in Fig. 4 served as the line standard. The TRL calibration placed the port 1 and port 2 calibration planes at the faces of the MEC DRWG straight sections ($z = 0$ and $z = h$ in Fig. 1), respectively. These calibration planes were then phase shifted to their desired locations at the front and back faces of the MUT by

$$\begin{aligned} S_{11}^{\text{meas}} &= S_{11}^{\text{VNA}} e^{\text{j}2k_{z0}\ell} \\ S_{21}^{\text{meas}} &= S_{21}^{\text{VNA}} e^{\text{j}k_{z0}(h-d)} \\ S_{12}^{\text{meas}} &= S_{12}^{\text{VNA}} e^{\text{j}k_{z0}(h-d)} \\ S_{22}^{\text{meas}} &= S_{22}^{\text{VNA}} e^{\text{j}2k_{z0}[h-(\ell+d)]}. \end{aligned} \tag{8}$$

Recall that ℓ was included in the development for error analysis purposes, i.e., to model the possibility that the front face of the MUT did not align with the calibration plane at $z = 0$. Every attempt was made to physically place the front face of the MUT at $z = 0$ and thereby make $\ell = 0$. It should be noted that sample-position error can be removed by using reference-plane-invariant formulations for the S-parameters [15] or for ε_r and μ_r directly [21]. Error in sample position was included in this analysis because the traditional Nicolson–Ross–Weir (NRW) [30], [31] ε_r and μ_r extraction technique utilized here is commonly used throughout industry and academia.

The ε_r and μ_r of FGM-125 were found by averaging the closed-form NRW forward (values computed from S_{11}^{meas} and S_{21}^{meas}) and reverse (values computed from S_{12}^{meas} and S_{22}^{meas}) results. Note that ε_r and μ_r were also found by minimizing the root-mean-square difference between $\boldsymbol{S}^{\text{thy}}$ (1) and $\boldsymbol{S}^{\text{meas}}$ (8) using the Levenberg–Marquardt algorithm [53], [54], i.e.,

$$\begin{pmatrix} \hat{\varepsilon}_r \\ \hat{\mu}_r \end{pmatrix} = \underset{\varepsilon_r,\, \mu_r \in C}{\arg\min} \left\| \boldsymbol{S}^{\text{thy}}(f; \varepsilon_r, \mu_r) - \boldsymbol{S}^{\text{meas}}(f) \right\|_2 \tag{9}$$

where $\boldsymbol{S} = \begin{pmatrix} S_{11} & S_{21} & S_{12} & S_{22} \end{pmatrix}^{\text{T}}$ and f is the frequency. The ε_r and μ_r results obtained by solving (9) were nearly identical to those yielded using NRW.

Using the specifications supplied by the WRD650 DRWG manufacturer given in [55] and reproduced in Table I[1] (see also Fig. 2), an extensive error analysis on the extracted values of ε_r and μ_r was performed. In addition to the tolerances on the DRWG dimensions given in Table I, the ε_r and μ_r errors due to uncertainties in sample position $\sigma_\ell = 0.05$ mm, sample thickness σ_d =0.05 mm, sample-holder length σ_h =0.05 mm, and measured S-parameters ($\sigma_{S_{ij}}$ given in [50]) were also considered. The following expression was used to calculate the measurement uncertainty in the real part of ε_r [15]:

$$\begin{aligned} \sigma_{\varepsilon_r^{\text{r}}}^2 = &\sum_{i,j=1}^{2} \left(\frac{\partial \varepsilon_r^{\text{r}}}{\partial S_{ij}^{\text{r}}} \sigma_{S_{ij}^{\text{r}}} \right)^2 + \sum_{i,j=1}^{2} \left(\frac{\partial \varepsilon_r^{\text{r}}}{\partial S_{ij}^{\text{i}}} \sigma_{S_{ij}^{\text{i}}} \right)^2 \\ &+ \left(\frac{\partial \varepsilon_r^{\text{r}}}{\partial d} \sigma_d \right)^2 + \left(\frac{\partial \varepsilon_r^{\text{r}}}{\partial \ell} \sigma_\ell \right)^2 + \left(\frac{\partial \varepsilon_r^{\text{r}}}{\partial h} \sigma_h \right)^2 \\ &+ \sum_{i=1}^{2} \left(\frac{\partial \varepsilon_r^{\text{r}}}{\partial k_c} \frac{\partial k_c}{\partial r_i} \sigma_{r_i} \right)^2 \\ &+ \left(\frac{\partial \varepsilon_r^{\text{r}}}{\partial k_c} \frac{\partial k_c}{\partial a} \sigma_a \right)^2 + \left(\frac{\partial \varepsilon_r^{\text{r}}}{\partial k_c} \frac{\partial k_c}{\partial b} \sigma_b \right)^2 \\ &+ \left(\frac{\partial \varepsilon_r^{\text{r}}}{\partial k_c} \frac{\partial k_c}{\partial \Delta x} \sigma_{\Delta x} \right)^2 + \left(\frac{\partial \varepsilon_r^{\text{r}}}{\partial k_c} \frac{\partial k_c}{\partial \Delta y} \sigma_{\Delta y} \right)^2 \end{aligned} \tag{10}$$

where the superscripts r and i denote the real and imaginary parts, respectively. The partial derivatives in the aforementioned expression were estimated using the central difference approximation. The values for $\sigma_{\varepsilon_r^{\text{i}}}$, $\sigma_{\mu_r^{\text{r}}}$, and $\sigma_{\mu_r^{\text{i}}}$ were calculated in a similar manner as earlier. Note that the error values provided by (10) are worst case estimates [15].

B. ECCOSORB® FGM-125 Results

Fig. 5 shows the ε_r [see Fig. 5(a)] and μ_r [see Fig. 5(b)] results for FGM-125 using the DRWG measurement system shown in Fig. 4. Provided to serve as a reference, the dashed black traces on the plots are the FGM-125 ε_r and μ_r results measured using three precision rectangular WG systems—C-band WR137 (5.85–8.2 GHz), X-band WR90 (8.2–12.4 GHz), and K_u-band WR62 (12.4–18 GHz). The bars on the plots represent the errors in the ε_r and μ_r measurements ($\pm 2\sigma_{\varepsilon_r}$ and $\pm 2\sigma_{\mu_r}$, respectively), calculating using (10), considering the MEC WRD650 DRWG dimensions and tolerances given in Table I as well as uncertainties in sample position, sample thickness, sample-holder length, and measured S-parameters. To demonstrate the overall impact that rounded DRWG aperture corners have on ε_r and μ_r, the results using k_c values found with the mode-matching (blue bars) and MFIE (red bars) methods are also shown. Fig. 6 shows the magnitudes of the sensitivity factors $\partial \varepsilon_r^{\text{r}} / \partial k_c$, $\partial \varepsilon_r^{\text{i}} / \partial k_c$, $\partial \mu_r^{\text{r}} / \partial k_c$, and $\partial \mu_r^{\text{i}} / \partial k_c$ versus frequency. Table II complements Fig. 6 by reporting the magnitudes of the DRWG dimension sensitivity factors which were calculated using the MFIE formulation method.

Considering the magnitudes reported in Table II, uncertainties in DRWG dimensions, especially uncertainty in Δy, can result in significant errors in ε_r and μ_r. To the authors' knowledge, this is the first time this analysis has been performed. Note that the magnitudes of the other error sources, namely, sample position, sample thickness, sample-holder length, and measured S-parameters, are not shown here for the sake of brevity. Analyses of those error sources can be found in numerous other references [2], [15], [18], [21], [56]–[59].

Overall, the results yielded by the DRWG system compare well with the reference results with the main exception being in the ε_r^{r} values. ECCOSORB® FGM-125 is sold in 30.48 cm $\times$ 30.48 cm $\times$ 3.12 mm sheets [49]. Significant variation in

[1]The value given for r_2 in [55] is 0.508 mm MAX. It was assumed that this meant a nominal value for r_2 = 0.254 mm with an uncertainty of σ_{r_2} = 0.254 mm.

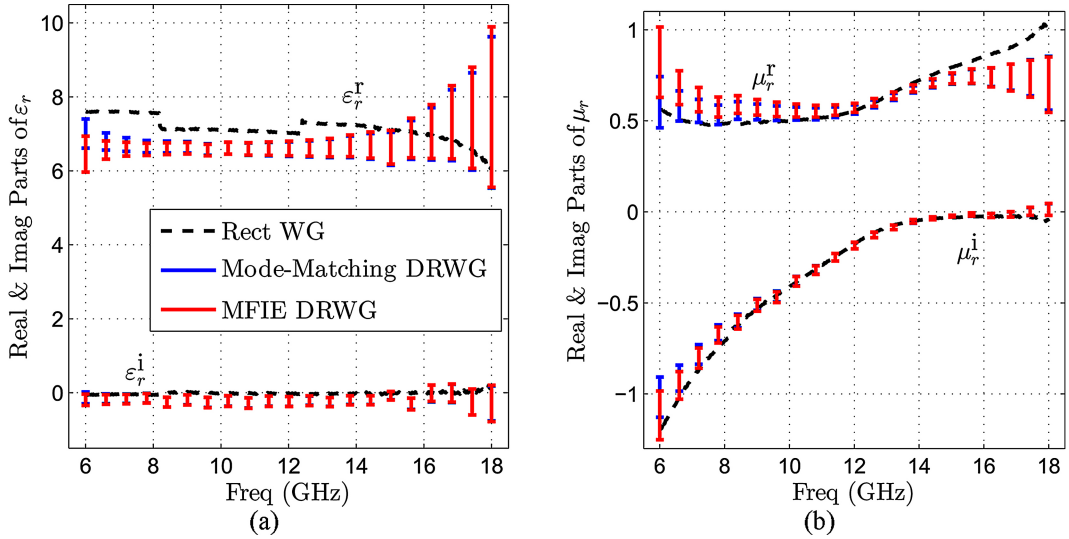

Fig. 5. (a) Relative complex permittivity ε_r results and (b) permeability μ_r results for FGM-125 using the DRWG measurement system shown in Fig. 4 and discussed in Section II. The dashed black traces on the plots are the FGM-125 ε_r and μ_r results measured using three precision rectangular WG systems—C-band WR137 (5.85–8.2 GHz), X-band WR90 (8.2–12.4 GHz), and K_u-band WR62 (12.4–18 GHz). These traces are provided to serve as a reference. The bars on the plots represent the errors in the ε_r and μ_r measurements ($\pm 2\sigma_{\varepsilon_r}$ and $\pm 2\sigma_{\mu_r}$) considering the MEC WRD650 DRWG dimensions and tolerances given in Table I as well as uncertainties in sample position $\sigma_\ell = 0.05$ mm, sample thickness σ_d =0.05 mm, sample-holder length σ_h =0.05 mm, and measured S-parameters (see [50] for $\sigma_{S_{ij}}$). The blue bars show the results utilizing k_c found using the mode-matching method; the red bars show the results utilizing k_c found using the MFIE technique.

FGM-125 $\varepsilon_r^{\mathrm{r}}$ values has been empirically noted from sheet to sheet and even from different locations on the same sheet. Typical values for FGM-125 $\varepsilon_r^{\mathrm{r}}$ range from 6.9–7.6; the manufacturer states that $\varepsilon_r^{\mathrm{r}} = 7$ [60].

The values and uncertainties in ε_r and μ_r obtained using the k_c values from the mode-matching (blue bars) and MFIE (red bars) methods are generally the same—the exception to this being at low frequencies. Recall that the mode-matching and MFIE methods differed in k_c values by approximately 3% for a rounded-corner DRWG aperture. At low frequencies, i.e., near cutoff, $k_c \approx k$ implying small k_z. It, therefore, makes sense that a 3% difference in the value of k_c would have a greater impact on ε_r and μ_r at lower frequencies than at higher frequencies where k_z approaches k.

C. Discussion

The true benefit of the proposed approach comes by contrasting the measurement requirements of the traditional rectangular WG system with those of the DRWG system. To obtain characterization data from 6–18 GHz using the traditional rectangular WG approach required three rectangular WG bands and three rectangular MUT samples for a total of 12 measurements (3 × thru, line, reflect, and MUT measurements). Furthermore, at the rectangular WG band edges, i.e., 8.2 and 12.4 GHz in Fig. 5(a) and (b), jumps in the ε_r and μ_r results are clearly evident caused by physically changing the measurement apparatus and recalibrating. Note that these jumps (especially conspicuous in the $\varepsilon_r^{\mathrm{r}}$ results) could also be caused by MUT inhomogeneity alluded to above. On the other hand, the DRWG approach required one DRWG band and one DRWG sample (four total measurements). Because of the broadband nature of DRWGs, the apparatus did not have to be changed and consistent ε_r and μ_r results were obtained over the whole frequency band. MUT sample preparation is more difficult using the proposed approach than the traditional rectangular WG method; however, the DRWG system requires a much smaller sample, making it an especially attractive measurement option for MUTs that are expensive to produce or procure. Note that while broadband characterization data like the results presented in Fig. 5 are certainly possible using coaxial, free-space, or stripline systems, as previously stated, accurate calibration and MUT preparation requirements are not as easily achieved (or not available) compared to the proposed DRWG system.

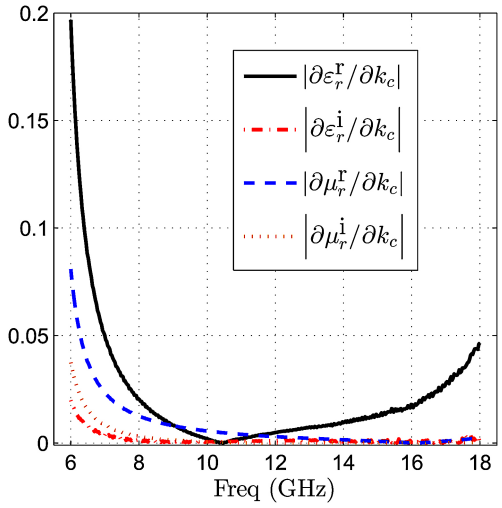

Fig. 6. Magnitudes of the sensitivity factors $\partial\varepsilon_r^{\mathrm{r}}/\partial k_c$, $\partial\varepsilon_r^{\mathrm{i}}/\partial k_c$, $\partial\mu_r^{\mathrm{r}}/\partial k_c$, and $\partial\mu_r^{\mathrm{i}}/\partial k_c$ versus frequency.

TABLE II
DRWG DIMENSION SENSITIVITY FACTORS

Sensitivity Factor	Magnitude ($\times 10^3$)
$\partial k_c/\partial a$	4.9631
$\partial k_c/\partial b$	6.7561
$\partial k_c/\partial \Delta x$	6.7955
$\partial k_c/\partial \Delta y$	33.819
$\partial k_c/\partial r_1$	3.9483
$\partial k_c/\partial r_2$	3.1343

IV. CONCLUSION

In this paper, a TR material characterization technique was presented which used DRWGs. The new DRWG measurement system offered broadband measurements and a simple and accurate calibration—combining many of the positive aspects of TEM-mode and rectangular WG systems. The derivation of the theoretical S-parameters, necessary for determining ε_r and μ_r of the MUT, was briefly discussed in Section II. The primary focus of Section II was to determine the cutoff wavenumber k_c of the DRWG since it determines the mode propagation constant critical in theoretical S-parameters computation. Two methods for determining k_c were presented. The first made use of the mode-matching technique and was applicable to DRWG apertures composed of right-angled corners. The other method made use of the surface equivalence principle and an MFIE formulation to determine k_c. Using this technique, it was possible to determine k_c for DRWGs with rounded corners—DRWG manufacturing process rounds the aperture corners—and thus, for the first time, assess what effect rounded DRWG corners have on ε_r and μ_r. Section III presented experimental material characterization results of a magnetic absorbing material comparing the results obtained using the proposed DRWG apparatus with those obtained using traditional rectangular WG measurements collected over three rectangular WG bands—C-band, X-band, and K_u-band. The proposed DRWG system yielded comparable results to the traditional rectangular WG approach, yet only required four measurements as opposed to 12. An extensive ε_r and μ_r error analysis was also performed accounting for manufacturer-specified DRWG design tolerances, i.e., aperture width, aperture height, gap width, gap height, and corner curvature, as well as uncertainties in sample position, sample thickness, sample-holder length, and measured S-parameters.

REFERENCES

[1] K. Sarabandi and F. Ulaby, "Technique for measuring the dielectric constant of thin materials," *IEEE Trans. Instrum. Meas.*, vol. 37, no. 4, pp. 631–636, Dec. 1988.

[2] M. Havrilla and D. Nyquist, "Electromagnetic characterization of layered materials via direct and de-embed methods," *IEEE Trans. Instrum. Meas.*, vol. 55, no. 1, pp. 158–163, Feb. 2006.

[3] F. Costa, "Surface impedance measurement of resistive coatings at microwave frequencies," *IEEE Trans. Instrum. Meas.*, vol. 62, no. 2, pp. 432–437, Feb. 2013.

[4] C. Wan, B. Nauwelaers, W. De Raedt, and M. Van Rossum, "Two new measurement methods for explicit determination of complex permittivity," *IEEE Trans. Microw. Theory Tech.*, vol. 46, no. 11, pp. 1614–1619, Nov. 1998.

[5] M. Hyde, M. Havrilla, and P. Crittenden, "A novel method for determining the R-card sheet impedance using the transmission coefficient measured in free-space or waveguide systems," *IEEE Trans. Instrum. Meas.*, vol. 58, no. 7, pp. 2228–2233, Jul. 2009.

[6] M. Janezic and J. Jargon, "Complex permittivity determination from propagation constant measurements," *IEEE Microw. Guided Wave Lett.*, vol. 9, no. 2, pp. 76–78, Feb. 1999.

[7] U. Hasar, "A new calibration-independent method for complex permittivity extraction of solid dielectric materials," *IEEE Microw. Wireless Compon. Lett.*, vol. 18, no. 12, pp. 788–790, Dec. 2008.

[8] U. C. Hasar. (2009). Thickness-independent automated constitutive parameters extraction of thin solid and liquid materials from microwave measurements. *PIER* [Online]. *92*, pp. 17–32. Available: http://ceta.mit.edu/pier/pier92/02.09031606.pdf

[9] U. C. Hasar and O. Simsek. (2009). On the application of microwave calibration-independent measurements for noninvasive thickness evaluation of medium- or low-loss solid materials. *PIER* [Online]. *91*, pp. 377–392. Available: http://ceta.mit.edu/pier/pier91/24.09020801.pdf

[10] U. Hasar, "Calibration-independent method for complex permittivity determination of liquid and granular materials," *Electron. Lett.*, vol. 44, no. 9, pp. 585–586, Apr. 2008.

[11] K.-H. Baek, H.-Y. Sung, and W. S. Park, "A 3-position transmission/reflection method for measuring the permittivity of low loss materials," *IEEE Microw. Guided Wave Lett.*, vol. 5, no. 1, pp. 3–5, Jan. 1995.

[12] R. A. Fenner, E. J. Rothwell, and L. L. Frasch. (2012, Jan.). A comprehensive analysis of free-space and guided-wave techniques for extracting the permeability and permittivity of materials using reflection-only measurements. *Radio Sci.* [Online]. *47(1)*, p. RS1004. Available: http://dx.doi.org/10.1029/2011RS004755

[13] M. Arai, J. Binner, and T. Cross, "Comparison of techniques for measuring high-temperature microwave permittivity: Measurements of alumina/zircona system," *J. Microw. Power Electromagn. Energy*, vol. 31, no. 1, pp. 12–18, 1996.

[14] M. Arai, J. Binner, and T. Cross, "Correction of errors due to airgaps for microwave complex permittivity measurement using a coaxial line," *Electron. Lett.*, vol. 31, no. 2, pp. 114–115, Jan. 1995.

[15] J. Baker-Jarvis, E. Vanzura, and W. Kissick, "Improved technique for determining complex permittivity with the transmission/reflection method," *IEEE Trans. Microw. Theory Tech.*, vol. 38, no. 8, pp. 1096–1103, Aug. 1990.

[16] A. Gorriti and E. Slob, "Comparison of the different reconstruction techniques of permittivity from S-parameters," *IEEE Trans. Geosci. Remote Sens.*, vol. 43, no. 9, pp. 2051–2057, Sep. 2005.

[17] A. Gorriti and E. Slob, "Synthesis of all known analytical permittivity reconstruction techniques of nonmagnetic materials from reflection and transmission measurements," *IEEE Trans. Geosci. Remote Sens.*, vol. 2, no. 4, pp. 433–436, Oct. 2005.

[18] A. Gorriti and E. Slob, "A new tool for accurate S-parameters measurements and permittivity reconstruction," *IEEE Trans. Geosci. Remote Sens.*, vol. 43, no. 8, pp. 1727–1735, Aug. 2005.

[19] C. Wan, B. Nauwelaers, W. De Raedt, and M. Van Rossum, "Complex permittivity measurement method based on asymmetry of reciprocal two-ports," *Electron. Lett.*, vol. 32, no. 16, pp. 1497–1498, Aug. 1996.

[20] N.-E. Belhadj-Tahar, A. Fourrier-Lamer, and H. de Chanterac, "Broadband simultaneous measurement of complex permittivity and permeability using a coaxial discontinuity," *IEEE Trans. Microw. Theory Tech.*, vol. 38, no. 1, pp. 1–7, Jan. 1990.

[21] K. Chalapat, K. Sarvala, J. Li, and G. Paraoanu, "Wideband reference-plane invariant method for measuring electromagnetic parameters of materials," *IEEE Trans. Microw. Theory Tech.*, vol. 57, no. 9, pp. 2257–2267, Sep. 2009.

[22] D. Ghodgaonkar, V. Varadan, and V. Varadan, "Free-space measurement of complex permittivity and complex permeability of magnetic materials at microwave frequencies," *IEEE Trans. Instrum. Meas.*, vol. 39, no. 2, pp. 387–394, Apr. 1990.

[23] V. Varadan, K. Jose, and V. Varadan, "In situ microwave characterization of nonplanar dielectric objects," *IEEE Trans. Microw. Theory Tech.*, vol. 48, no. 3, pp. 388–394, Mar. 2000.

[24] G. Hanson, J. Grimm, and D. Nyquist, "An improved de-embedding technique for the measurement of the complex constitutive parameters of materials using a stripline field applicator," *IEEE Trans. Instrum. Meas.*, vol. 42, no. 3, pp. 740–745, Jun. 1993.

[25] W. Barry, "A broad-band, automated, stripline technique for the simultaneous measurement of complex permittivity and permeability," *IEEE Trans. Microw. Theory Tech.*, vol. 34, no. 1, pp. 80–84, Jan. 1986.

[26] L. F. Chen, C. K. Ong, C. P. Neo, V. V. Varadan, and V. K. Varadan, *Microwave Electronics: Measurement and Materials Characterization*. West Sussex, U.K.: Wiley, 2004.

[27] G. F. Engen and C. A. Hoer, "Thru-reflect-line: An improved technique for calibrating the dual six-port automatic network analyzer," *IEEE Trans. Microw. Theory Tech.*, vol. 27, no. 12, pp. 987–993, Dec. 1979.
[28] J. Montgomery, "On the complete eigenvalue solution of ridged waveguide," *IEEE Trans. Microw. Theory Tech.*, vol. 19, no. 6, pp. 547–555, Jun. 1971.
[29] W. Sun and C. Balanis, "MFIE analysis and design of ridged waveguides," *IEEE Trans. Microw. Theory Tech.*, vol. 41, no. 11, pp. 1965–1971, Nov. 1993.
[30] A. M. Nicolson and G. F. Ross, "Measurement of the intrinsic properties of materials by time-domain techniques," *IEEE Trans. Instrum. Meas.*, vol. 19, no. 4, pp. 377–382, Nov. 1970.
[31] W. B. Weir, "Automatic measurement of complex dielectric constant and permeability at microwave frequencies," *Proc. IEEE*, vol. 62, no. 1, pp. 33–36, Jan. 1974.
[32] Y. H. Cho and H. J. Eom. (2001). Fourier transform analysis of a ridge waveguide and a rectangular coaxial line. *Radio Sci.* [Online]. *36(4)*, pp. 533–538. Available: http://dx.doi.org/10.1029/2000RS002381
[33] S. Hopfer, "The design of ridged waveguides," *IRE Trans. Microw. Theory Tech.*, vol. 3, no. 5, pp. 20–29, Oct. 1955.
[34] J. Pyle, "The cutoff wavelength of the TE_{10} mode in ridged rectangular waveguide of any aspect ratio," *IEEE Trans. Microw. Theory Tech.*, vol. 14, no. 4, pp. 175–183, Apr. 1966.
[35] Y. Utsumi, "Variational analysis of ridged waveguide modes," *IEEE Trans. Microw. Theory Tech.*, vol. 33, no. 2, pp. 111–120, Feb. 1985.
[36] J. Helszajn, *Ridge Waveguide and Passive Microwave Components*. London, U.K.: The Institute of Electrical Engineers, 2000.
[37] R. S. Elliot, *An Introduction to Guided Waves and Microwave Circuits*. Englewood Cliffs, NJ, USA: Prentice-Hall, 1993.
[38] Y. Rong and K. Zaki, "Characteristics of generalized rectangular and circular ridge waveguides," *IEEE Trans. Microw. Theory Tech.*, vol. 48, no. 2, pp. 258–265, Feb. 2000.
[39] R. E. Collin, *Field Theory of Guided Waves*, 2nd ed. New York, NY, USA: IEEE Press, 1991.
[40] R. Harrington, *Time-Harmonic Electromagnetic Fields*. Piscataway, NJ, USA: IEEE Press, 2001.
[41] A. Wexler, "Solution of waveguide discontinuities by modal analysis," *IEEE Trans. Microw. Theory Tech.*, vol. 15, no. 9, pp. 508–517, Sep. 1967.
[42] M. Swaminathan, E. Arvas, T. Sarkar, and A. Djordjevic, "Computation of cutoff wavenumbers of TE and TM modes in waveguides of arbitrary cross sections using a surface integral formulation," *IEEE Trans. Microw. Theory Tech.*, vol. 38, no. 2, pp. 154–159, Feb. 1990.
[43] M. Swaminathan, T. Sarkar, and A. Adams, "Computation of TM and TE modes in waveguides based on a surface integral formulation," *IEEE Trans. Microw. Theory Tech.*, vol. 40, no. 2, pp. 285–297, Feb. 1992.
[44] C. Kim, S. Yu, R. Harrington, J. Ra, and S. Lee, "Computation of waveguide modes for waveguides of arbitrary cross-section," *IEE Proc. H: Microw., Antennas Propag.*, vol. 137, no. 2, pp. 145–149, Apr. 1990.
[45] K.-M. Chen, "A mathematical formulation of the equivalence principle," *IEEE Trans. Microw. Theory Tech.*, vol. 37, no. 10, pp. 1576–1581, Oct. 1989.
[46] A. F. Peterson, S. L. Ray, and R. Mittra, *Computational Methods for Electromagnetics*. New York, NY, USA: IEEE Press, 1998.
[47] W. Sun and C. Balanis, "Analysis and design of quadruple-ridged waveguides," *IEEE Trans. Microw. Theory Tech.*, vol. 42, no. 12, pp. 2201–2207, Dec. 1994.
[48] R. Harrington, *Field Computation by Moment Methods*. New York, NY, USA: IEEE Press, 1993.
[49] Emerson & Cuming Microwave Products, Inc. (2012, Apr.). ECCOSORB® FGM thin, flexible, impervious, broadband absorbers [Online]. Available: http://www.eccosorb.com/Collateral/Documents/English-US/FGM.pdf
[50] Agilent Technologies, Inc., "Technical specifications Agilent Techologies PNA series network analyzers E8362B/C, E8363B/C, and E8364B/C," 2008.
[51] Microwave Engineering Corporation. Double-ridge waveguide-to-coaxial adapters R40 series [Online]. Available: http://www.microwaveeng.com/catalog/t7e.pdf
[52] Microwave Engineering Corporation. Double-ridge straight sections, bends and twists R10 R120 R130 R150 series [Online]. Available: http://www.microwaveeng.com/catalog/t34e.pdf
[53] K. Levenberg, "A method for the solution of certain problems in least squares," *Quart. Appl. Math.*, vol. 2, pp. 164–168, 1944.
[54] D. Marquardt. (1963). An algorithm for least-squares estimation of nonlinear parameters. *SIAM J. Appl. Math.* [Online]. *11(2)*, pp. 431–441. Available: http://epubs.siam.org/doi/abs/10.1137/0111030
[55] Microwave Engineering Corporation. Double-ridge & MEC flatguide flanges & Waveguide [Online]. Available: http://www.microwaveeng.com/catalog/t22d.pdf
[56] S. S. Agili, A. W. Morales, J. Li, and M. Resso, "Finding the probability distribution functions of S-parameters and their Monte Carlo simulation," *IEEE Trans. Instrum. Meas.*, vol. 61, no. 11, pp. 2993–3002, Nov. 2012.
[57] E. Ni, "An uncertainty analysis for the measurement of intrinsic properties of materials by the combined transmission-reflection method," *IEEE Trans. Instrum. Meas.*, vol. 41, no. 4, pp. 495–499, Aug. 1992.
[58] D. Sjöberg and C. Larsson, "Cramér Rao bounds for determination of permittivity and permeability in slabs," *IEEE Trans. Microw. Theory Tech.*, vol. 59, no. 11, pp. 2970–2977, Nov. 2011.
[59] C. Larsson, D. Sjöberg, and L. Elmkvist, "Waveguide measurements of the permittivity and permeability at temperatures of up to 1000°C," *IEEE Trans. Instrum. Meas.*, vol. 60, no. 8, pp. 2872–2880, Aug. 2011.
[60] Emerson & Cuming Microwave Products, Inc. (2007, Aug.). ECCOSORB® FGM permittivity & permeability data [Online]. Available: http://www.eccosorb.com/Collateral/Documents/English-US/Electricalrameters/FGM

Milo W. Hyde IV (S'10–M'10–SM'12) received the B.S. degree in computer engineering from the Georgia Institute of Technology, Atlanta, GA, USA, in 2001, and the M.S. and Ph.D. degrees in electrical engineering from the Air Force Institute of Technology, Wright–Patterson Air Force Base, Dayton, OH, USA, in 2006 and 2010, respectively.

From 2001 to 2004, he was a Maintenance Officer with the F-117A Nighthawk, Holloman Air Force Base, Alamogordo, NM, USA. From 2006 to 2007, he was a Government Researcher with the Air Force Research Laboratory, Wright–Patterson Air Force Base. He is currently an Assistant Professor with the Department of Electrical and Computer Engineering, Air Force Institute of Technology, Wright-Patterson Air Force Base. His current research interests include electromagnetic material characterization, guided-wave theory, scattering, and optics.

Dr. Hyde is a member of the International Society for Optical Engineering and the Optical Society of America.

Michael J. Havrilla (S'85–M'86–SM'05) received the B.S. degree in physics and mathematics, the M.S.E.E degree, and the Ph.D. degree in electrical engineering from Michigan State University, East Lansing, MI, USA in 1987, 1989 and 2001 respectively.

From 1990 to 1995, he was with General Electric Aircraft Engines, Evendale, OH, USA, and Lockheed Skunk Works, Palmdale, CA, USA, where he was an Electrical Engineer. He is currently a Professor with the Department of Electrical and Computer Engineering, Air Force Institute of Technology, Wright-Patterson Air Force Base, Dayton, OH, USA. His current research interests include electromagnetic and guided-wave theory, electromagnetic propagation and radiation in complex media and structures, and electromagnetic materials characterization.

Dr. Havrilla is a member of the International Union of Radio Science Commission B and the Eta Kappa Nu honor society.

Andrew E. Bogle (S'04—M'07) received the B.S., M.S., and Ph.D. degrees in electrical engineering from Michigan State University, East Lansing, MI, USA, in 2001, 2004, and 2007, respectively.

From 2007 to 2009, he was an Electrical Engineer with Niowave Inc., Lansing, MI, USA. He is currently a Research Engineer with the Sensor Systems Division, University of Dayton Research Institute, Dayton, OH, USA. He is also with the Department of Electrical and Computer Engineering, Air Force Institute of Technology, Wright-Patterson Air Force Base, Dayton, OH, USA. His current research interests include electromagnetic materials characterization, electromagnetic and guided-wave theory, and electromagnetic propagation and radiation in complex media and structures.

Nathan J. Lehman received the B.S. degree in electrical engineering from the University of Nevada, Las Vegas, NV, USA, in 2008. He is currently pursuing the M.S. degree in electrical engineering with the Air Force Institute of Technology, Wright-Patterson Air Force Base, Dayton, OH, USA.

From 2008 to 2010, he was an Operations Engineer with the Airborne Laser program, Edwards AFB, CA, USA. From 2010 to 2011, he was an Executive Officer at U.S. Air Force Test Pilot School. His current research interests include electromagnetic material characterization, radar, and infrared technology.